

## Article

# Germanium Dioxide Nanoparticles Mitigate Biochemical and Molecular Changes Characterizing Alzheimer's Disease in Rats

Sara A. Abdel Gaber <sup>1,\*</sup>, Amal H. Hamza <sup>2</sup>, Mohamed A. Tantawy <sup>3,4</sup>, Eman A. Toraih <sup>5</sup>  
and Hanaa H. Ahmed <sup>3,4</sup>

<sup>1</sup> Nanomedicine Department, Institute of Nanoscience and Nanotechnology, Kafrelsheikh University, Kafr El Sheikh 33516, Egypt

<sup>2</sup> Biochemistry and Nutrition Department, Faculty of Women, Ain Shams University, Cairo 11566, Egypt

<sup>3</sup> Hormones Department, Medical Research and Clinical Studies Institute, National Research Center, Dokki, Giza 12622, Egypt

<sup>4</sup> Stem Cell Lab, left of Excellence for Advanced Sciences, National Research Centre, Dokki, Giza 12622, Egypt

<sup>5</sup> Genetics Unit, Histology and Cell Biology Department, Faculty of Medicine, Suez Canal University, Ismailia 41522, Egypt

\* Correspondence: sara\_mohamed@nano.kfs.edu.eg

**Abstract:** Alzheimer's disease (AD) is a neurodegenerative disorder that jeopardizes the lives of diagnosed patients at late stages. This study aimed to assess, for the first time, the efficiency of germanium dioxide nanoparticles (GeO<sub>2</sub>NPs) in mitigating AD at the in vivo level compared to cerium dioxide nanoparticles (CeO<sub>2</sub>NPs). Nanoparticles were synthesized using the co-precipitation method. Their antioxidant activity was tested. For the bio-assessment, rats were randomly assigned into four groups: AD + GeO<sub>2</sub>NPs, AD + CeO<sub>2</sub>NPs, AD, and control. Serum and brain tau protein, phosphorylated tau, neurogranin, amyloid  $\beta$  peptide 1-42, acetylcholinesterase, and monoamine oxidase levels were measured. Brain histopathological evaluation was conducted. Furthermore, nine AD-related microRNAs were quantified. Nanoparticles were spherical with diameters ranging from 12–27 nm. GeO<sub>2</sub>NPs exhibited a stronger antioxidant activity than CeO<sub>2</sub>NPs. Serum and tissue analyses revealed the regression of AD biomarkers to almost control values upon treatment using GeO<sub>2</sub>NPs. Histopathological observations strongly supported the biochemical outcomes. Then, miR-29a-3p was down-regulated in the GeO<sub>2</sub>NPs-treated group. This pre-clinical study substantiated the scientific evidence favoring the pharmacological application of GeO<sub>2</sub>NPs and CeO<sub>2</sub>NPs in AD treatment. Our study is the first report on the efficiency of GeO<sub>2</sub>NPs in managing AD. Further studies are needed to fully understand their mechanism of action.

**Keywords:** Alzheimer's disease; germanium dioxide nanoparticles; cerium dioxide nanoparticles; MicroRNAs; antioxidant; Alzheimer's biomarkers



**Citation:** Abdel Gaber, S.A.; Hamza, A.H.; Tantawy, M.A.; Toraih, E.A.; Ahmed, H.H. Germanium Dioxide Nanoparticles Mitigate Biochemical and Molecular Changes Characterizing Alzheimer's Disease in Rats. *Pharmaceutics* **2023**, *15*, 1386. <https://doi.org/10.3390/pharmaceutics15051386>

Academic Editor: Tania Limongi

Received: 10 December 2022

Revised: 9 February 2023

Accepted: 27 April 2023

Published: 30 April 2023



**Copyright:** © 2023 by the authors. Licensee MDPI, Basel, Switzerland. This article is an open access article distributed under the terms and conditions of the Creative Commons Attribution (CC BY) license (<https://creativecommons.org/licenses/by/4.0/>).

## 1. Introduction

Alzheimer's disease (AD) is one of the most common neurodegenerative illnesses, resulting in gradual dementia in the elderly population [1]. It represents the fifth-leading cause of mortality, with a prevalence of more than 46 million globally, according to AD International Recordings [2]. Although the specific causation is still unknown, many validated studies proved that AD is caused by a mix of hereditary and environmental factors. Several previous studies indicate that the accumulation of toxic proteins, specifically tau tangles and amyloid  $\beta$  peptide (A $\beta$ ) plaques, and their movement in and out of brain neurons, serve as primary mechanisms for the onset of AD [3]. Thus, AD is distinguished by intracellular neurofibrillary tangles (NFTs) and extracellular senile A $\beta$  plaques in the brain. NFTs are abnormally hyperphosphorylated microtubules linked together by the tau protein [4]. Only the A $\beta$  cascade and tau hyperphosphorylation hypotheses have gained prevalent approval for the diagnosis of AD [5].

Promising studies showed the role of small non-coding microRNAs as diagnostic, prognostic, and predictive biomarkers in AD and miRNA combinations increase the sensitivity and specificity compared with single miRNAs [6]. Thus, miRNAs are particularly abundant in the neurological system, where they perform a role in neuronal activities, such as neurite outgrowth, dendritic spine architecture, neuronal development, and synaptic plasticity [7]. Of these, cerebrospinal fluid (CSF) miR-125b-5p, miR-146a-5p, and miR-29a-3p levels were a better ancillary panel to A $\beta$  1-42: Total-tau ratio that differentiates between AD and controls [6].

A panel of 10 microRNAs, including miR-107, miR-146a, and miR-125b, was deregulated early in AD, nearly 20 years before the onset of clinical symptoms [8]. Dysregulation of miR-9a-5p was found to be associated with altered brain-enriched gene expression patterns that, in part, characterize AD neuropathology [9]. Some miRNAs have steadily been deregulated in cellular and animal AD models. It has been shown that voluntary physical exercise modulates the expression of several miRNAs involved in AD, such as miR-30a-5p and miR-128, in a spontaneous senescence-accelerated P8 (SAMP8) mouse model [10]. Down-regulation of miR-181c-5p in the hippocampus of SAMP8 mice is also known to perform a role in AD pathogenesis [11]. These microRNAs can be used as candidate biomarkers in clinical practice, assisting in identifying novel proteins and pathways linked to AD, and they may reveal novel future therapeutic targets for AD. Currently, the treatment modalities aim to relieve the symptoms and delay the disease progression. The available medications authorized by the FDA are cholinesterase inhibitors, which raise acetylcholine concentrations and, thereby, neurotransmitter activity [12].

Alternative and cutting-edge treatments, such as nanomedicine, have been suggested for AD. In this regard, nanoparticles displaying free radical scavenging properties and antioxidant activity, such as cerium dioxide nanoparticles (CeO<sub>2</sub>NPs), are of great interest. Several studies have reported that CeO<sub>2</sub>NPs are free radical scavengers in vitro and in vivo [13]. CeO<sub>2</sub>NPs shuttle between their 3p and 4p states, and oxidation of Ce4p to Ce3p causes oxygen niches and defects on the surface of the crystalline lattice structure, producing a circumstance for the occurrence of redox reactions. As a result, CeO<sub>2</sub>NPs mimic the catalytic activities of several antioxidant enzymes [14]. Additionally, CeO<sub>2</sub>NPs are widely used in treating medical disorders caused by reactive oxygen intermediates due to their unique redox properties [15].

Germanium is a naturally occurring nonessential element. The biomedical implementations of germanium are so limited [16], but it has been shown that germanium has anti-cancer and anti-viral properties in vivo and antitumor, anti-aging, and anti-inflammatory properties in vivo and in vitro. Furthermore, organic germanium compounds effectively improve immune function in different pathological conditions in preclinical studies [17]. In addition, germanium is effective against liver diseases, hypertension, arthritis, food allergies, autoimmune diseases, senile osteoporosis, and malaria [16]. Various enzymes have been reported to be inhibited by germanium, including alcohol dehydrogenase, glutamic oxaloacetic transaminase, glutathione-S-transferase, and lactic dehydrogenase [18]. Germanium dioxide nanoparticles (GeO<sub>2</sub>NPs) became the focus of many studies that aimed to control their shape [19] and synthesize them in reverse micelles [20]. Their applications so far are limited to photocatalytic degradation [21,22], radiosensitization [23] use in lithium batteries [24,25], and photoluminescence sensing [26,27].

This study aimed to investigate, for the first time, the efficacy of GeO<sub>2</sub>NPs in alleviating AD induced in the experimental animals. CeO<sub>2</sub>NPs were used for the comparison. To fulfill this goal, both nanoparticles were synthesized, fully characterized, and tested for their antioxidant activity. AD biochemical and molecular relevant markers of treated rats were quantified to fully understand the possible mechanism of action. Brain tissue pathology was also studied to confirm our hypothesis that GeO<sub>2</sub>NPs could protect brain cells from damage in an AD animal model and a set of possibly involved miRNAs were studied.

## 2. Materials and Methods

### 2.1. Chemicals

Germanium tetrachloride ( $\text{GeCl}_4$ ), 2,2-Diphenyl-1-picrylhydrazyl (DPPH), and (2,2'-azino-bis(3-ethylbenzothiazoline-6-sulfonic acid)) (ABTS) were purchased from Sigma Aldrich, St. Louis, MO, USA. Acetyl acetone ( $\text{C}_5\text{H}_8\text{O}_2$ ) and ethylene glycol ( $\text{C}_2\text{H}_6\text{O}_2$ ) were obtained from Alfa Aesar, Karlsruhe, Germany. Cerium nitrate hexahydrate ( $\text{Ce}(\text{NO}_3)_3 \cdot 6\text{H}_2\text{O}$ ) with 99% purity was supplied from Chemlab, Zedelgem, Belgium. NaOH and  $\text{AlCl}_3$  were acquired from El-Gomhouria for Chemicals, Ramadan City, Egypt. All other reagents, solvents, and chemicals used for analysis met the quality criteria of the international standards.

### 2.2. Synthesis of Germanium Dioxide Nanoparticles ( $\text{GeO}_2\text{NPs}$ )

$\text{GeO}_2\text{NPs}$  were synthesized as previously described [28] with some modifications. In brief, acetylacetone (10 mL) and ethylene glycol (10 mL) were properly mixed. Then,  $\text{GeCl}_4$  in a molar ratio of 1:4 to the mixture was added dropwise under magnetic stirring upon which a gel was formed, and 15 mL of distilled water was added to the reaction in a dropwise manner while stirring. The reaction was left for 4 h at 150 °C. The obtained white precipitate was collected by centrifugation and washed twice using distilled water. The obtained nanoparticles were then washed using ethanol and left in the oven at 50 °C overnight to dry.  $\text{GeO}_2\text{NPs}$  powder was then calcinated in a furnace adjusted to 400 °C for 4 h.

### 2.3. Synthesis of Cerium Dioxide Nanoparticles ( $\text{CeO}_2\text{NPs}$ )

$\text{CeO}_2\text{NPs}$  were synthesized using the precipitation method as described previously [29]. Briefly, 10 mL of 0.3 M NaOH was added dropwise to a stirring 10 mL of 0.1 M cerium nitrate hexahydrate  $\text{Ce}(\text{NO}_3)_3 \cdot 6\text{H}_2\text{O}$ . The reaction mixture was left stirring for 6 h in a water bath maintained at 70 °C. The formed precipitate was collected by centrifugation. At least three cycles of washing using distilled water were performed. The precipitate was washed once with absolute ethanol and left at 60 °C until completely dry. Annealing was conducted using a furnace at 400 °C for 4 h.

### 2.4. Characterization of $\text{GeO}_2\text{NPs}$ and $\text{CeO}_2\text{NPs}$

X-ray powder diffraction (XRD) was conducted after annealing to verify phase purity according to the  $2\theta$  range of 10–80° with a scan rate of 8°  $\text{min}^{-1}$  (Philips X Pert diffractometer). Morphologically, they were characterized using high-resolution transmission electron microscopy (HR-TEM) using JEOL (JEM-2100, Osaka, Japan) at an accelerating voltage of 200 kV. Fourier transmission infrared (FTIR) spectroscopy was conducted (Model no. 4000, JASCO, Tokyo, Japan) with a range of 400–4000  $\text{cm}^{-1}$  using KBr pellets. The surface charge was measured using the Malvern Zeta sizer Nano ZS instrument (Malvern Instruments, Malvern, UK). At least three measurements were performed [30].

### 2.5. Assessment of $\text{GeO}_2\text{NPs}$ and $\text{CeO}_2\text{NPs}$ Ex-Vivo Antioxidant Activity

The radical scavenging activity of the synthesized nanoparticles was quantified using both 2,2-Diphenyl-1-picrylhydrazyl (DPPH) and (2,2'-azino-bis(3-ethylbenzothiazoline-6-sulfonic acid)) (ABTS) assays. Vitamin C was the reference positive control in both assays. A serial dilution (10–100  $\mu\text{g}/\text{mL}$ ) of nanoparticles suspended in phosphate-buffered saline (PBS) was prepared by 15 min sonication in a water bath. In the DPPH assay, nanoparticle solution was mixed with an equal volume of DPPH solution (0.05  $\text{mg}/\text{mL}$ ) dissolved in methanol and the mixture was incubated in darkness for 2 h. The absorbance of the reaction mixture was measured at 517 nm using Shimadzu UV-2450 double beam spectrophotometer [30]. In the ABTS assay, radicals of ABTS were freshly prepared by mixing 7 mM of ABTS with 2.45 mM of potassium persulfate and incubating the mixture overnight in darkness. Nanoparticle solution was mixed with an equal volume of the prepared ABTS radical solution and absorbance was measured at 734 nm [31]. Measurements were

conducted in triplicates and results were expressed as % of inhibition calculated according to Equation (1).

$$\text{Inhibition(\%)} = \frac{A_c - A_s}{A_c} \times 100 \quad (1)$$

where  $A_c$  was the absorbance of the working solution free of nanoparticles and  $A_s$  was the absorbance of the working solution mixed with the nanoparticles. From the plotted curves, the concentration needed to scavenge 50% of the produced radical (IC50) was determined [32].

## 2.6. Biological Experiment

Physiologically, estrogen levels change significantly during the menstrual cycle, as estrogen level elevates during the mid-follicular phase, then decrease after ovulation, followed by a second increase during mid-luteal phase, and subsequently decrease at the end of menstrual cycle. Since, estrogens have neuroprotective function against AD [3], this fluctuation in hormones level might influence the treatment in female experimental AD model. Apparently, due to the mentioned fact, and to avoid any bias associated with this hormonal imbalance, we established our AD-treated model in adult male Wistar albino rats according to the established protocols.

### 2.6.1. Animals

Adult male *Wistar* albino rats weighing 200–220 g were procured from the Animal Care Unit at the National Research Centre, Cairo, Egypt. Food and water were available ad libitum. The room's temperature was maintained at  $20 \pm 2$  °C, and a 12:12 h light/dark cycle was sustained. The adaptation lasted at least one week before the initiation of the experimental protocol. Animal handling and management were following the Guidelines for the Animal Care and Use of the Ethical Committee for Medical Research of the National Research Centre, Egypt obtained in July 2021 with the approval number 1416072021.

### 2.6.2. Assessment of NPs Toxicity and In Vivo Antioxidant Activity

Rats were randomly grouped into three groups ( $n = 4$ ). The first group was the control that received PBS. The second group was the GeO<sub>2</sub>NPs group that received (37.5 mg/kg body weight) [33], and the third was the CeO<sub>2</sub>NPs group that received (0.5 mg/kg body weight) [34]. Treatment was administered as an intraperitoneal injection once weekly for 6 weeks. The vitality of rats was recorded, and rats were observed for signs of toxicity, such as behavioral changes, loss of weight, or excessive itching [35]. At the end of the treatment duration, rats were euthanized, and brain tissues were collected. The antioxidant whole brain homogenate levels of reduced glutathione (GSH) and superoxide dismutase (SOD) were measured using colorimetric activity assays [30]. Part of the tissues were paraformaldehyde fixed. The tissues were embedded in paraffin after dehydration. Sections were cut and mounted on glass slides. Immunohistochemical assessments of viability using Ki67 (Sigma Aldrich, USA) and the expression of Nrf2 (Santa Cruz Laboratory, Santa Cruz, CA, USA) were conducted [36]. Hematoxylin counterstaining was applied and the reactions sites of cerebellum, striatum, hippocampal dentate gyrus (DG), hippocampal prefrontal cortex (PL), and cerebral cortex were visualized as brown precipitates.

### 2.6.3. Induction of AD

AD was induced via oral administration of AlCl<sub>3</sub> dissolved in water (17 mg/kg body weight) for 6 weeks (5 days/week) [37].

#### 2.6.4. Experimental Protocol

Rats were randomly assigned into four groups ( $n = 10$ ). Group 1 (AD + GeO<sub>2</sub>NPs): The AD group was treated with GeO<sub>2</sub>NPs dissolved in PBS that were intraperitoneally administered once weekly (37.5 mg/kg body weight) for 6 weeks [33]. Group 2 (AD + CeO<sub>2</sub>NPs): The AD group was treated with CeO<sub>2</sub>NPs dissolved in PBS intraperitoneally administered once weekly (0.5 mg/kg body weight) for 6 weeks [34]. Group 3 was an AD-induced group that was left untreated. Group 4 (control group) served as a negative control of healthy rats and was intraperitoneally injected with vehicle (PBS) once weekly for 6 weeks. Of note, the nanoparticles before administration were sonicated in a water bath for 10 min before injection to avoid aggregation phenomena due to the high temperatures reached during the calcination process. At the end of the experimental period, all rats were allowed to fast overnight, and blood samples were drained from the tail vein, following light anesthesia, to obtain sera samples. After centrifugation at  $1800 \times g$  for 10 min at 4 °C, serum samples were cryopreserved in aliquots for analysis of biochemical markers. After blood collection, the rats were sacrificed, and brain tissues were harvested and thoroughly washed with PBS. The whole brain of a certain number of animals in each group was dissected and divided sagittally into two portions: The first portion was immediately collected in *RNAlater* RNA Stabilizing Reagent (Qiagen, Cat. No 76104, Germantown, MD, USA) and the homogenization of brain specimens was conducted. Then, total RNA, including miRNA, was extracted from the brain tissues of the four groups using Qiagen miRNeasy Kit (Qiagen, Catalog no. 217004) and stored at  $-80$  °C for downstream molecular analysis. The second portion of brain tissues was weighed and immediately homogenized to give 10% ( $w/v$ ) homogenate containing 50 mM Tris-HCl and 300 mM sucrose, pH 7.4 [38]. The brain homogenates were centrifuged at  $1800 \times g$  for 10 min at 4 °C. A supernatant (10%) was stored in aliquots at  $-20$  °C for the different biochemical determinations. Total protein concentration was also estimated to express the concentration of various biochemical parameters as  $\text{mg}^{-1}$  or  $\mu\text{g}^{-1}$  protein [39]. The whole brain of the remaining animals in each group was fixed in 10% formalin buffer for 24 h for the histological procedure.

#### 2.6.5. Biochemical Analyses (Serum and Brain)

Tau protein, phospho-tau protein, neurogranin (NG), and A $\beta$  peptide 1-42 levels, and acetylcholinesterase (AChE) and monoamine oxidase (MAO) activities, were measured in serum and brain homogenate by enzyme-linked immunosorbent assay (ELISA) using kits purchased from Glory Science Co., Ltd., Del Rio, TX, USA according to operating instructions.

#### 2.6.6. Quantitative Analysis of microRNAs Expression

The purity and concentration of RNA were recorded using a NanoDrop spectrophotometer at the wavelength-dependent extinction coefficient 33 (NanoDrop Tech., Inc., Wilmington, DE, USA). Total RNA (10 ng) was converted to cDNA using Archive High-Capacity Reverse Transcription kit (Applied Biosystems, Waltham, MA, USA, Catalog no. 4368814) in T-Professional Basic Biometra PCR System (Biometra, Goettingen, Germany). For microRNA detection, specific forward primers for nine miRNAs (miRNA-9, miRNA-16, miRNA-29, miRNA-107, miRNA-125, miRNA-128, miRNA-137, miRNA-146, and miRNA-181) and a universal reverse primer 5'-GAACATGTCTGCGTATCTC-3' were selected and retrieved from ORIGINE company (<https://www.origene.com/catalog/> accessed on 5 November 2021, Table 1). Runs of qPCR were performed using Maxima<sup>TM</sup> SYBR Green/ROX qPCR Master Mix (2X) (Thermo Fisher Scientific, Waltham, MA, USA, Catalog no. K0221), and beta-actin was used as an endogenous control. Appropriate negative and positive controls were also added. Real-time PCR reactions were carried out in StepOne<sup>TM</sup> Real-Time PCR System (Applied Biosystems) following the minimum information for publication of quantitative real-time PCR experiments (MIQE) guidelines. The results obtained were expressed in the quantification cycle (C<sub>q</sub>), and the relative expression of each tested miRNA was assessed according to the formula ( $2^{-\Delta\Delta C_t}$ ) [40,41].

**Table 1.** Primer sequences of the analyzed microRNAs. List of forward primers for the analyzed microRNAs.

microRNAs	The Sequence of Forwarding Primers
rno-miR-9a-5p	5'-TCTTTGGTTATCTAGCTGTAT-3'
rno-miR-16-5p	5'-TAGCAGCACGTAAATATTGG-3'
rno-miR-29a-3p	5'-ACTGATTTCTTTTGGTGTTTC-3'
rno-miR-107-5p	5'-AGCTTCTTTACAGTGTTCCT-3'
rno-miR-125b-5p	5'-TCCCTGAGACCCCTAATTGT-3'
rno-miR-128-2-5p	5'-GGGGGCCGATGCACTGTAA-3'
rno-miR-137-3p	5'-ACGGGTATTCTTGGGGTGGAT-3'
rno-miR-146a-5p	5'-TGAGAACTGAATCCATGGG-3'
rno-miR-181c-5p	5'-CATTCAACCTGTCCGGTGA-3'

### 2.6.7. Histopathological Procedure

Brain tissues were fixed in 10% buffered formalin for 24 h and washed with tap water. For dehydration, serial dilutions of ethyl alcohol were applied, after which, the specimens were cleared in xylene and processed using the paraffin wax embedding technique in a hot air oven at 56 °C for 6 h. Paraffin wax tissue blocks were sectioned using microtome at 4 microns thickness. Sections were collected on glass slides, deparaffinized, and stained for routine histological examination using hematoxylin and eosin (H&E) staining [36]. The histological sections were examined using an Olympus optical microscope (Tokyo, Japan).

### 2.7. Statistical Analysis

Statistical Package for the Social Sciences (SPSS) version 25 and Graph Pad Prism version 9.1.2 were used for analysis. Results are expressed as mean  $\pm$  standard error of the mean (SE). One-way analysis of variance (ANOVA) was followed by the least significant difference (LSD) and Tukey tests for multiple comparisons. Two-sided  $p < 0.05$  was considered statistically significant.

## 3. Results

### 3.1. Morphological Features of the Synthesized GeO<sub>2</sub>NPs and CeO<sub>2</sub>NPs and Their Ex-Vivo Antioxidant Activity

The synthesized GeO<sub>2</sub>NPs and CeO<sub>2</sub>NPs were imaged using a high-resolution transmission electron microscope (HR-TEM) to examine their morphological appearance. As seen in (Figure 1a), GeO<sub>2</sub>NPs were quasi-spherical in shape with an average diameter of 20 nm. From the magnified HR-TEM image in (Figure 1b), the lattice structure of the nanoparticles was clearly detected, which confirmed their crystalline nature. The marked interplanar (d) spacing of 0.27 nm was for the plane (011), which was the prominent one. As shown in (Figure 1c), the synthesized CeO<sub>2</sub>NPs were 12–15 nm in diameter with a spherical shape. Typical metal oxide aggregation was observed. In the magnified HR-TEM (Figure 1d), the lattice structure of the nanoparticles was obvious. Based on this, a spacing of 0.29 nm was measured, which suggested that the synthesized CeO<sub>2</sub>NPs had a face-lefted cubic fluorite crystallographic structure.

Radical scavenging activity of GeO<sub>2</sub>NPs and CeO<sub>2</sub>NPs was confirmed by DPPH and APTS assays using vitamin C as a standard. According to the results of the DPPH assay (Supplementary Materials, Figure S1a), and APTS assay (Figure S1b), both nanoparticles exerted an antioxidant activity that was significantly weaker than vitamin C. Both nanoparticles showed a similar antioxidant activity when their concentrations were below 60  $\mu\text{g}/\text{mL}$ . At higher concentrations, GeO<sub>2</sub>NPs activity was stronger than CeO<sub>2</sub>NPs. The concentrations needed to scavenge 50% of DPPH (DPPH IC<sub>50</sub>) of GeO<sub>2</sub>NPs was  $55.1 \pm 0.3 \mu\text{g}/\text{mL}$  while DPPH IC<sub>50</sub> of CeO<sub>2</sub>NPs was  $79.1 \pm 0.4 \mu\text{g}/\text{mL}$  (Figure 1e). Similarly, APTS IC<sub>50</sub> of

GeO<sub>2</sub>NPs ( $65.4 \pm 0.3 \mu\text{g}/\text{mL}$ ) was lower than the respective one of CeO<sub>2</sub>NPs ( $91.7 \pm 0.6$ ) as seen in (Figure 1d).

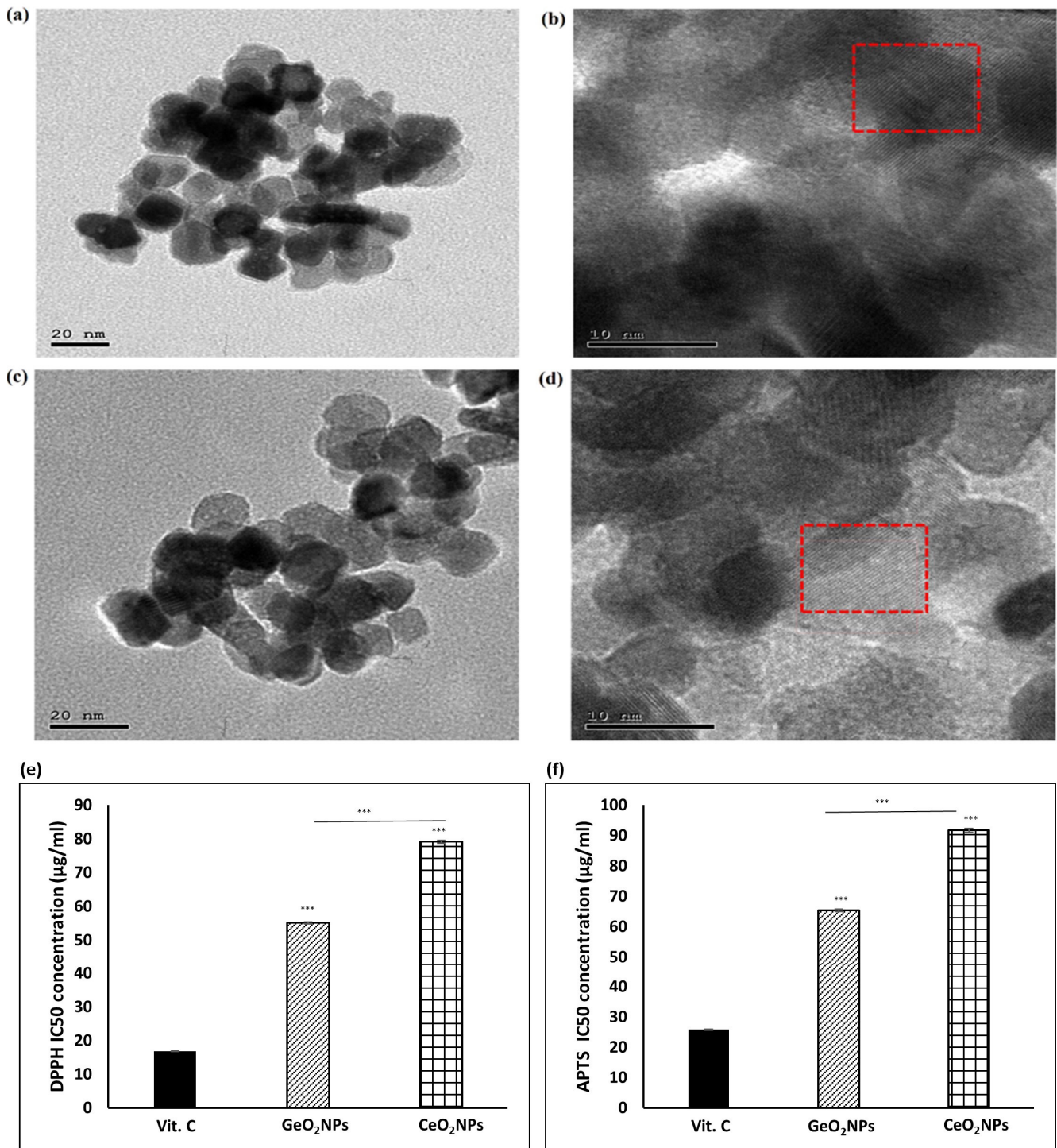


**Figure 1.** (a) High-resolution transmission electron microscope (HR-TEM) representative image of synthesized GeO<sub>2</sub>NPs, (b) a magnified HR-TEM image of GeO<sub>2</sub>NPs showing the lattice structure as indicated in the red rectangle, (c) HR-TEM representative image of synthesized CeO<sub>2</sub>NPs, (d) a magnified HR-TEM image of CeO<sub>2</sub>NPs showing the lattice structure as indicated in the red rectangle, (e) DPPH IC<sub>50</sub> of GeO<sub>2</sub>NPs and CeO<sub>2</sub>NPs, (f) APTS IC<sub>50</sub> of GeO<sub>2</sub>NPs and CeO<sub>2</sub>NPs. Vitamin C (Vit C) was used as a standard. ( $n = 3$ , \*\*\* depicts  $p \leq 0.001$ ).

### 3.2. XRD Pattern, FTIR, and Zeta Potential of the Synthesized GeO<sub>2</sub>NPs and CeO<sub>2</sub>NPs

The synthesized GeO<sub>2</sub>NPs were examined for their purity and crystallinity. The respective X-ray diffractogram (XRD) is shown in (Figure 2a). Results revealed that the synthesized nanoparticles were crystalline and show a pure hexagonal phase (space group: P32 2 1). The calculated cell parameters were a: 4.9113 Å and c: 5.6009 Å. There was a close matching with JCPDS No. 85-0473. The calculated average crystalline size applying the Scherrer equation was 24 nm. Selected area electron diffraction (SAED), shown in (Figure 2b), demonstrated the polycrystalline nature of the nanoparticles. By applying Bragg's equation, the equivalent diffraction angles were 27°, 45°, and 53°. The XRD pattern of calcinated CeO<sub>2</sub>NPs is shown in (Figure 2c). The major high-intensity peaks were observed at 28°, 33°, 47°, and 56°, respectively, corresponding to the 111, 200, 220, and 311 crystal planes. Some minor peaks were also observed. The existence of those diffraction peaks matched the standard JCPDS data card (34-0394) for cerium oxide. The prepared CeO<sub>2</sub>NPs exhibited a pure face-lefted cubic polycrystalline structure as indicated by the sharp narrow and intense peaks. The calculated nanocrystalline particle size using the Debye Scherrer equation was 15 nm. SAED patterns presented in (Figure 2d) showed the polycrystalline nature of the nanoparticles. The corresponding interplanar spacing (d) was calculated following Bragg's equation to be 0.325, 0.2717, 0.1941, and 0.1645 nm from the inner to the outer circle, respectively. They corresponded to 2θ 27.2, 32.5, 45.5, and 53.7°, respectively. Their respective miller indexations were 111, 200, 220, and 311. Thus, for both nanoparticles, the characteristic 2 theta degrees recorded in XRD analysis agreed with those calculated from the SAED pattern.

Both annealed GeO<sub>2</sub>NPs and CeO<sub>2</sub>NPs were examined by FTIR. The results for GeO<sub>2</sub>NPs are shown in (Figure 2e). The well-reported GeO<sub>2</sub> characteristic bands [26,28] were observed. The first was the triplet band at 580, 550, and 510 cm<sup>-1</sup>, which corresponded to symmetric Ge-OH stretching, and the second was at 870 cm<sup>-1</sup>, which corresponded to GeO-Ge antisymmetric stretching. The band observed at 3500 to 3000 cm<sup>-1</sup> was assigned to OH groups of adsorbed water molecules. The weak band at 1650 cm<sup>-1</sup> was assigned to the bending vibration of water molecules and could also be assigned to -CO stretching vibration of carbonyl groups of the used organic solvents. FTIR results of CeO<sub>2</sub>NPs are shown in (Figure 2f). Peaks at 501 and 857 cm<sup>-1</sup> were assigned to Ce-O bonds [42]. The signal at 1567 cm<sup>-1</sup> was assigned to H-O-H bending vibration, which suggests that water molecules were adsorbed on the surface of the synthesized CeO<sub>2</sub>NPs [43]. A broad strong band at 3435 cm<sup>-1</sup> was present. This band was assigned to the OH stretching of chemisorbed hydroxyl groups on the surface of the nanoparticles. Furthermore, the peaks at 1487 and 1367 cm<sup>-1</sup> were assigned to νs (CO<sub>3</sub>) and δ (HO) modes of chemisorbed bicarbonate [44].

The zeta potentials of both nanoparticles were measured. GeO<sub>2</sub>NPs had an average surface charge of  $-27 \pm 2$  mV, while the surface charge of CeO<sub>2</sub>NPs was  $-17.5 \pm 1.4$  mV.

### 3.3. Safety of GeO<sub>2</sub>NPs and CeO<sub>2</sub>NPs and Their In Vivo Antioxidant Activity

During the entire treatment duration that lasted for 6 weeks, treated rats did not show mortality or signs of abnormal behavior that might indicate toxicity. The brain section of both GeO<sub>2</sub>NPs and CeO<sub>2</sub>NPs treated rats were positive to Ki67 (Figure 3a) confirming the safety of the selected doses. Tissue sections were positive to Nrf2 (Figure 3b) and tissue levels of GSH (Figure 3c) and SOD (Figure 3d) were significantly higher in treated groups than in the control ( $p < 0.05$ ).

### 3.4. Serum Biochemical AD-Relevant Markers in Response to Treatments

Upon administration of AlCl<sub>3</sub> in the AD group, the serum levels of tau protein and phosphorylated tau were 2-fold and 3.6-fold higher than the control group, respectively, while the serum level of neurogranin (NG) declined to half of the control, confirming the success of the AD model (Table 2). Treating AD-bearing rats with CeO<sub>2</sub>NPs resulted in significant depletion ( $p < 0.05$ ) in serum tau protein and phosphorylated tau accompanied

by significant elevation ( $p < 0.05$ ) in the NG serum level versus the AD-bearing rats, indicating their therapeutic efficacy. On the other hand, the AD-bearing rats treated with  $\text{GeO}_2\text{NPs}$  had tau protein and NG levels similar to the control group and phosphorylated tau markedly lower than the group treated with  $\text{CeO}_2\text{NPs}$ .

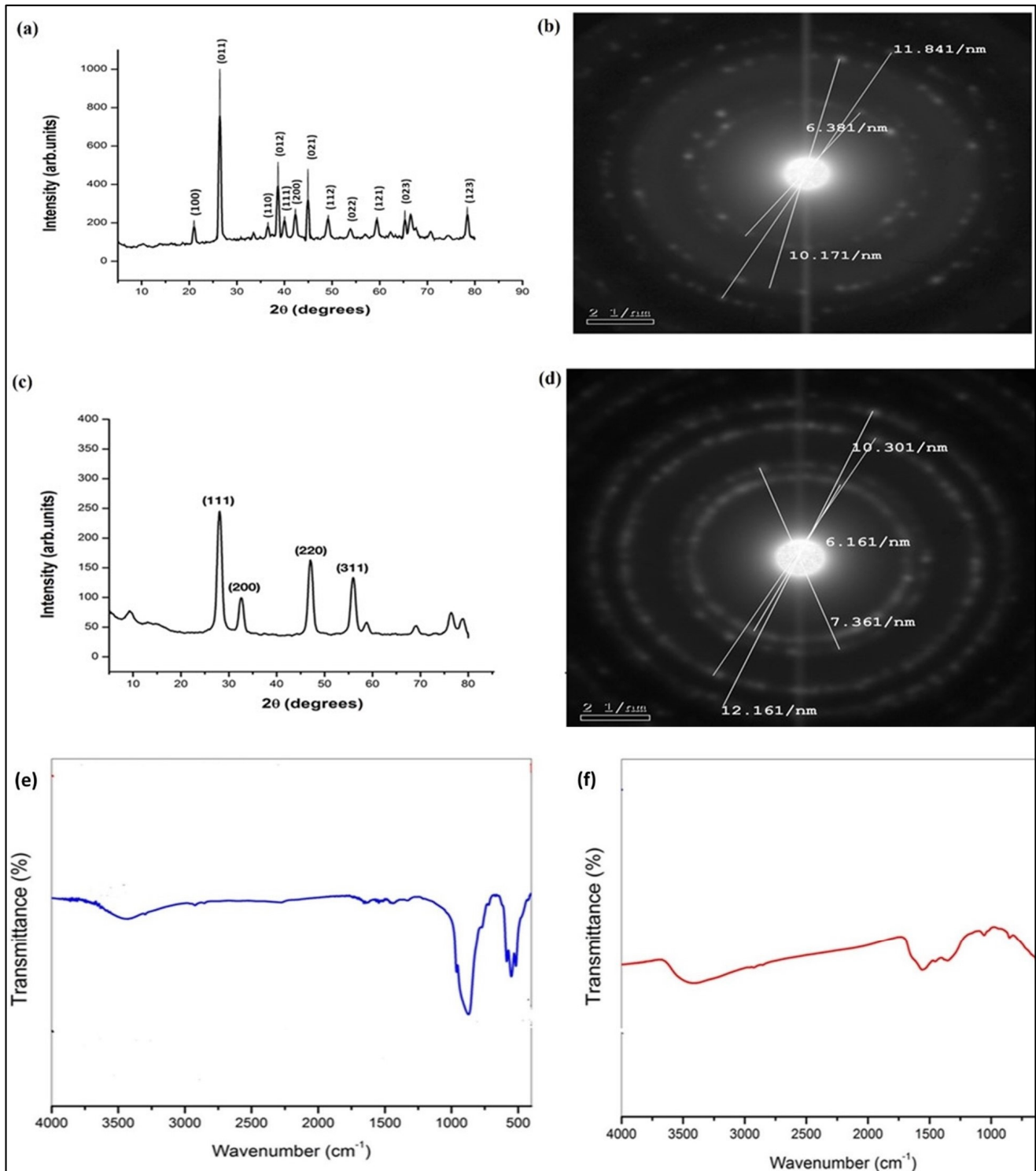


**Figure 2.** (a)  $\text{GeO}_2\text{NPs}$  XRD pattern, (b)  $\text{GeO}_2\text{NPs}$  selected area electron diffraction (SAED), (c)  $\text{CeO}_2\text{NPs}$  XRD pattern, (d)  $\text{CeO}_2\text{NPs}$  SAED, (e) FTIR spectrum of  $\text{GeO}_2\text{NPs}$ , (f) FTIR spectrum of  $\text{CeO}_2\text{NPs}$ .

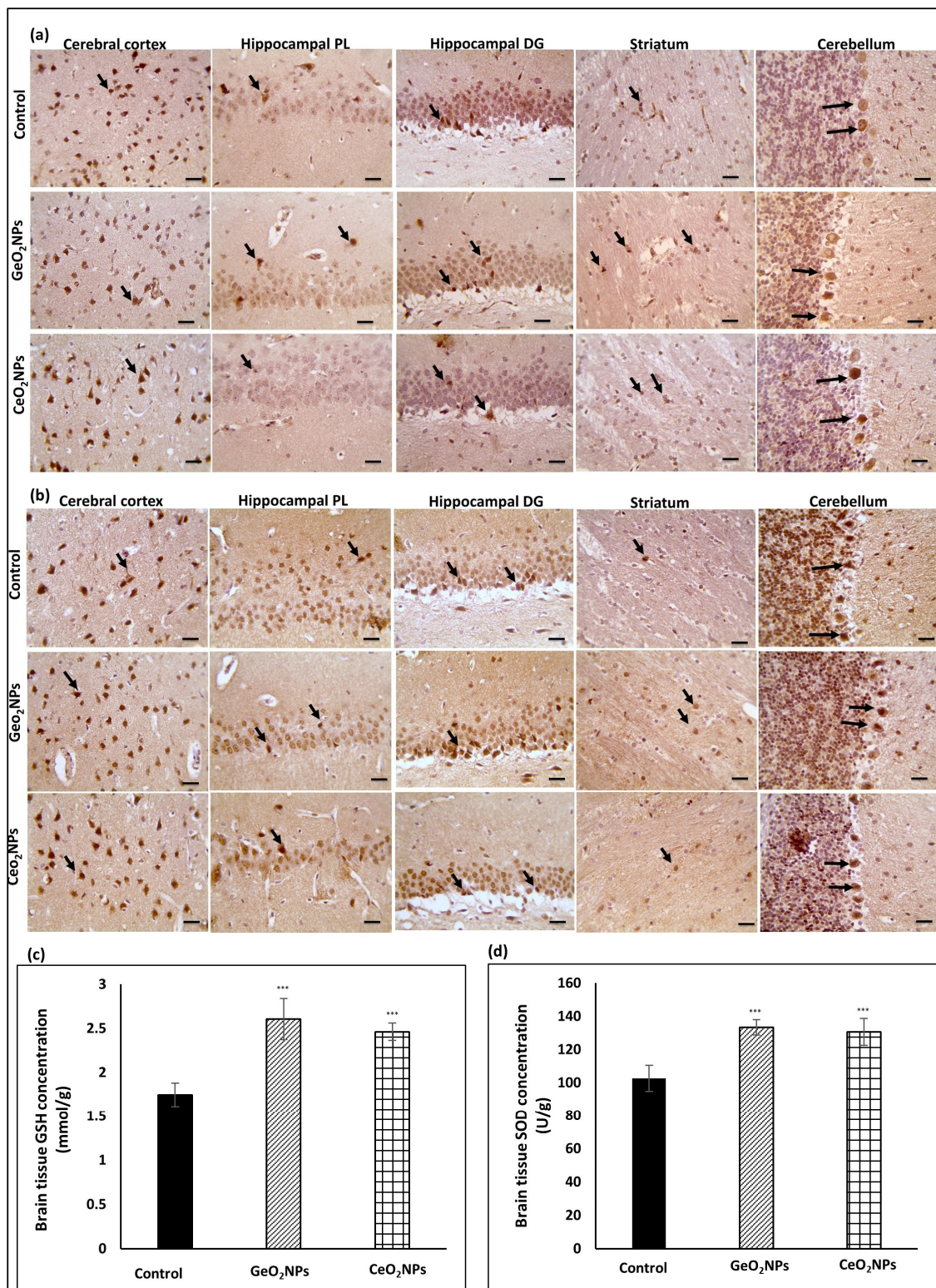


**Figure 3.** (a) Representative immunohistochemical photographs of control, GeO<sub>2</sub>NPs and CeO<sub>2</sub>NPs treated rats showing brain cerebellum, striatum, hippocampal dentate gyrus (DG), hippocampal prelimbic cortex (PL), and cerebral cortex stained with Ki67, (b) stained with Nrf2 antibody. Magnification was 400× and bar is 50 μm. Black arrows depicted positive regions for the applied antibodies, (c) brain tissue concentration of GSH, (d) brain tissue concentration of SOD. Experiments were repeated three times, presented are average and standard deviation, \*\*\* indicated *p* value < 0.001.

**Table 2.** Measured biomarkers in serum. Serum tau, phospho-tau protein, neurogranin (NG), A $\beta$  peptide 1-42, acetylcholinesterase (AChE), and Monoamine oxidase (MAO) in the experimental groups (Mean  $\pm$  SE).

Marker	AD + GeO <sub>2</sub> NPs	AD + CeO <sub>2</sub> NPs	AD	Control
Tau protein pg/mL	280 $\pm$ 9 *	348 $\pm$ 8 *	449 $\pm$ 8 *	220 $\pm$ 9
Phospho Tau pg/mL	75 $\pm$ 3	108 $\pm$ 5 *	171 $\pm$ 10 *	48 $\pm$ 5
Neurogranin (NG) ng/mL	1.22 $\pm$ 0.05	0.99 $\pm$ 0.04 *	0.67 $\pm$ 0.04 *	1.40 $\pm$ 0.05
A $\beta$ peptide 1-42 pg/mL	14.9 $\pm$ 0.5 *	13.3 $\pm$ 0.4 *	11.5 $\pm$ 0.4 *	20.3 $\pm$ 0.7
Acetylcholinesterase (AChE) ng/mL	198 $\pm$ 4 *	253 $\pm$ 2 *	313 $\pm$ 3 *	113 $\pm$ 3
Monoamine oxidase (MAO) pg/mL	1868 $\pm$ 40 *	2796 $\pm$ 37 *	3372 $\pm$ 32 *	1815 $\pm$ 23

\* Significant change at  $p > 0.05$  in comparison with control and/or AD-induced group.

In the AD group, the activities of serum acetylcholinesterase (AChE) and monoamine oxidase (MAO) were 3-fold and 2-fold higher than in the control group, respectively, whereas serum levels of A $\beta$  peptide 1-42 were reduced by half (Table 2). Treating AD-bearing rats with CeO<sub>2</sub>NPs significantly ( $p < 0.05$ ) reduced AChE and MAO activities in contrast to the AD-bearing rats, but their values were still higher than controls. On the other hand, treating AD-bearing rats with GeO<sub>2</sub>NPs reduced serum AChE and MAO activities remarkably less than those in CeO<sub>2</sub>NPs-treated rats, where the values were similar to controls. In both treatment groups (AD + CeO<sub>2</sub>NPs and AD + GeO<sub>2</sub>NPs), serum A $\beta$  peptide 1-42 level significantly increased ( $p < 0.05$ ) compared to the AD-bearing group, but it was higher in the GeO<sub>2</sub>NPs-treated group than the CeO<sub>2</sub>NPs-treated group.

### 3.5. Brain Biochemical AD-Relevant Markers in Response to Treatments

Brain tau protein and phosphorylated tau levels were 2-fold and 2.7-fold higher in the AD group relative to controls, respectively, while brain NG level was significantly diminished ( $p < 0.05$ ) in the AD group versus the control group. These biomarkers were restored almost to control levels in the AD-bearing rats treated with GeO<sub>2</sub>NPs. In this regard, GeO<sub>2</sub>NPs showed a more prominent effect than CeO<sub>2</sub>NPs (Table 3).

**Table 3.** Measured biomarkers in tissue. Brain tau, phospho-tau protein, neurogranin (NG), A $\beta$  peptide 1-42, acetylcholinesterase (AChE), and Monoamine oxidase (MAO) in the experimental groups (Mean  $\pm$  SE).

Marker	AD + GeO <sub>2</sub> NPs	AD + CeO <sub>2</sub> NPs	AD	Control
Tau protein ng/ $\mu$ g protein	17.7 $\pm$ 0.3	21.5 $\pm$ 0.4 *	26.6 $\pm$ 0.7 *	14.6 $\pm$ 0.5
Phospho -Tau pg/ $\mu$ g protein	185 $\pm$ 4	264 $\pm$ 2 *	380 $\pm$ 4 *	140 $\pm$ 3
Neurogranin (NG) ng/mg protein	470 $\pm$ 7	419 $\pm$ 3 *	368 $\pm$ 2 *	535 $\pm$ 5
A $\beta$ peptide 1-42 ng/ $\mu$ g protein	10.6 $\pm$ 0.3 *	14.3 $\pm$ 0.2 *	16.9 $\pm$ 0.2 *	7.5 $\pm$ 0.4

**Table 3.** *Cont.*

Marker	AD + GeO <sub>2</sub> NPs	AD + CeO <sub>2</sub> NPs	AD	Control
Acetylcholinesterase (AChE) U/mg protein	595 ± 9 *	705 ± 4 *	790 ± 2 *	553 ± 4
Monoamine oxidase (MAO) nmol/mg protein	60.7 ± 0.7 *	68.3 ± 0.7 *	81.4 ± 1.0 *	52.4 ± 1.4

\* Significant change at  $p > 0.05$  in comparison with control and/or AD-induced group.

Brain A $\beta$  peptide level, AChE, and MAO activities showed significant elevation ( $p < 0.05$ ) in AD-bearing rats when compared with the control counterparts. Treatment of AD-bearing rats with either CeO<sub>2</sub>NPs or GeO<sub>2</sub>NPs brought about significant regression ( $p < 0.05$ ) in these markers in comparison with AD-bearing rats. Of note, GeO<sub>2</sub>NPs displayed a more pronounced impact than CeO<sub>2</sub>NPs regarding these parameters (Table 3).

### 3.6. Histopathological Observations

Brain sections of the rat groups were stained with H&E and examined for their histopathological features. In the four groups, the hippocampus, cerebellum, and brain cortex were investigated. The (Figure 4). The AD group treated with GeO<sub>2</sub>NPs was the only one showing a normal feature of pyramidal cells and neurons of the hippocampus whereas the AD treated group with CeO<sub>2</sub>NPs showed advanced degeneration and necrosis of neurons and pyramidal cells. The degradation and necrosis were aggravated and diffused in the AD group. Cerebellum of GeO<sub>2</sub>NPs and CeO<sub>2</sub>NPs treated groups showed degeneration and necrobiosis of Purkinje cells. Furthermore, cells of the granular area showed gliosis and degeneration and clump together. However, it is worth mentioning that those histopathological features were milder than the observed ones in the AD group. The brain cortex of GeO<sub>2</sub>NPs and CeO<sub>2</sub>NPs treated AD-induced rats showed necrosis of neurons. The recovery process and immune response were evident by the observed proliferation of astrocyte and microglial cells. The AD group showed necrobiosis of neurons and diffused neurofibrillary tangles. The control group showed normal histopathological features.

### 3.7. MicroRNAs Transcriptomic Signature

A literature search and bioinformatics analysis using mirPath v.3 KEGG reverse search (<http://snf-515788.vm.okeanos.grnet.gr/>) accessed on 5 November 2021 for AD KEGG pathway (rno05010) revealed nine putative AD-related microRNAs: rno-miR-9a-5p, rno-miR-16-5p, rno-miR-29a-3p, rno-miR-107-5p, rno-miR-125b-5p, rno-miR-128-2-5p, rno-miR-137-3p, rno-miR-146a-5p, and rno-miR-181c-5p. Using real-time PCR, we assessed the expression of these nine miRNAs in brain tissue from treated and non-treated AD groups (Figure 5). There was no significant difference in microRNAs expression between AD and control animals; however, miR-29a-3p was significantly down-regulated in the GeO<sub>2</sub>NPs-treated group compared to the AD group ( $p = 0.0080$ ).

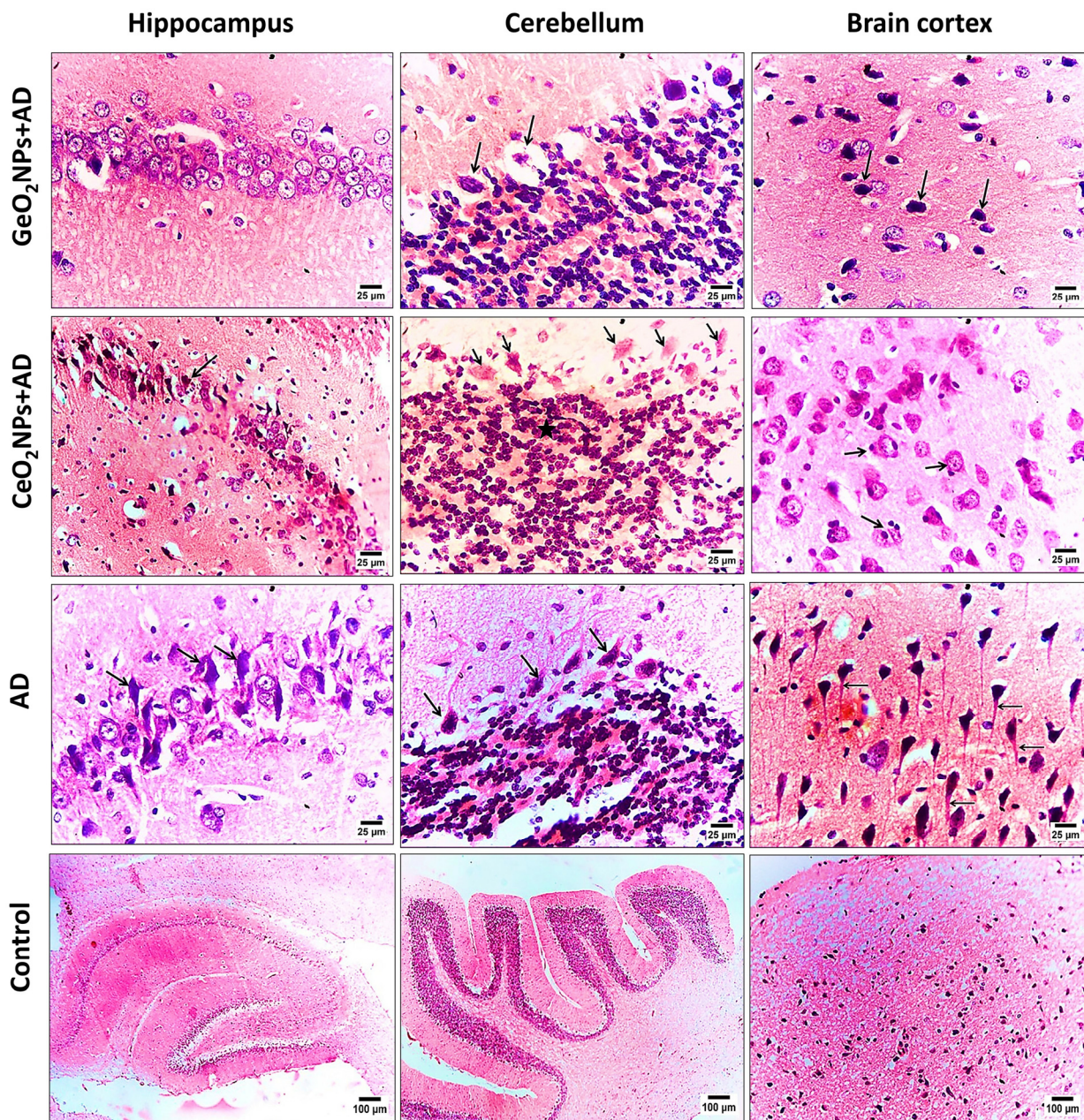


**Figure 4.** Photomicrograph of H&E-stained hippocampus, cerebellum, and brain cortex sections of AD-induced rats treated with  $\text{GeO}_2\text{NPs}$  (AD +  $\text{GeO}_2\text{NPs}$ ), treated with  $\text{CeO}_2\text{NPs}$  (AD +  $\text{CeO}_2\text{NPs}$ ), left untreated (AD) and healthy rats (Control). Arrows depicted degeneration and necrosis of neurons and arrows in the brain section of AD group depicted diffused neurofibrillary tangles. The star in the cerebellum section of  $\text{CeO}_2\text{NPs}$  + AD group depicts where the cells of granular area had gliosis, degeneration, and clumps together. Magnification was  $400\times$  in all samples except in the sections of the control where it was  $40\times$ .

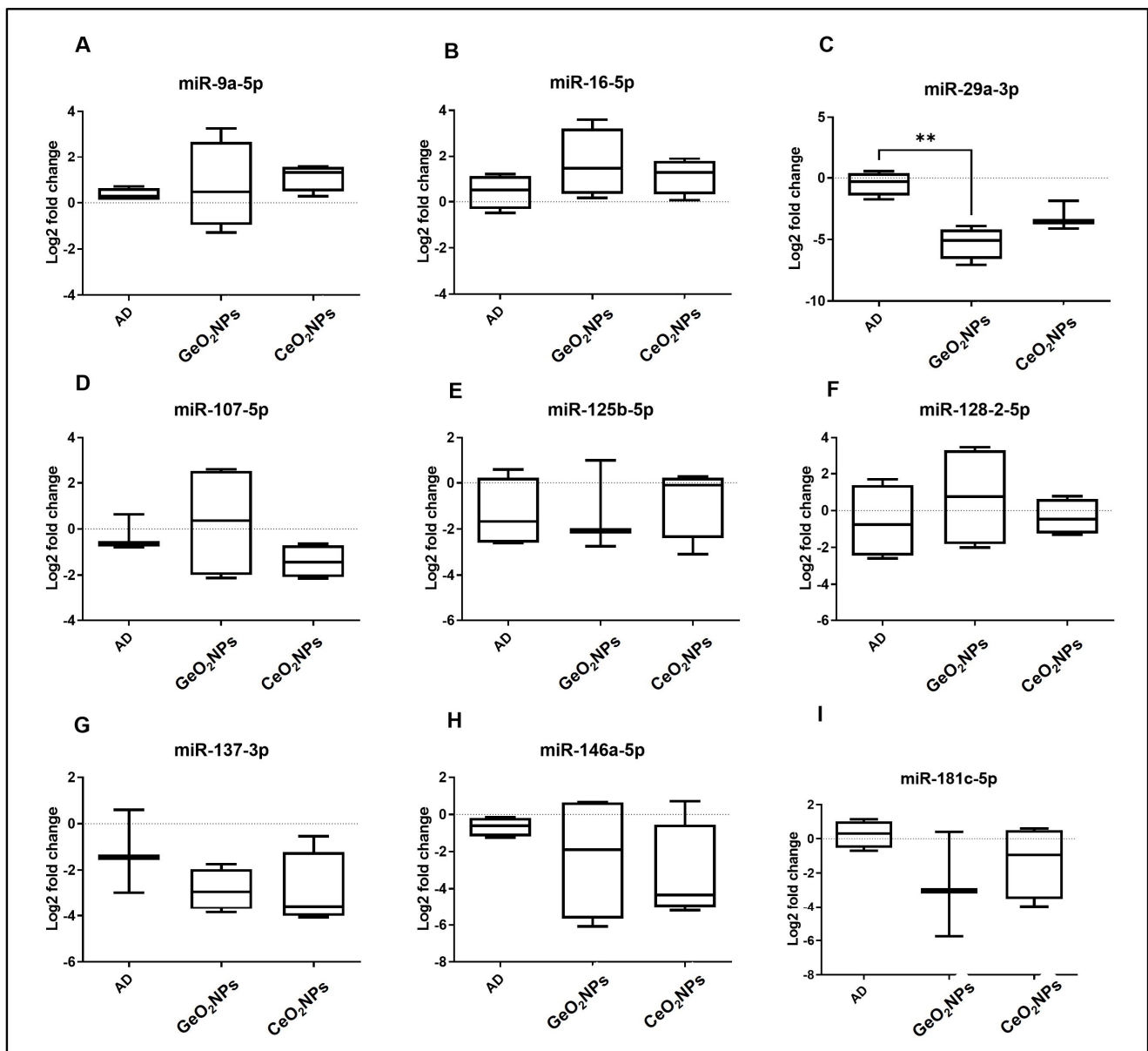


**Figure 5.** MicroRNA quantification in brain tissues of rats; AD, GeO<sub>2</sub>NPs-treated group, and CeO<sub>2</sub>NPs-treated group. The logarithmic transformation value of log 2-fold changes is shown. One-way ANOVA followed by post hoc Tukey tests were used. \*\*  $p < 0.01$ .

#### 4. Discussion

The main purpose of this study was to assess for the first time the potential therapeutic effect of GeO<sub>2</sub>NPs compared to CeO<sub>2</sub>NPs in an experimental model of AD. GeO<sub>2</sub>NPs and CeO<sub>2</sub>NPs were synthesized using a facile co-precipitation synthetic method. Unlike other methods, co-precipitation can be easily optimized. Adjusting the temperature, reaction time, and the ratio between acetylacetone and germanium tetrachloride could alter the size of the produced GeO<sub>2</sub>NPs [28].

Similarly, for the synthesis of CeO<sub>2</sub>NPs, numerous methods have been reported. One is the sonochemical method [45]. In this study, the precipitation method was selected since it is facile and easily scalable, unlike others requiring high pressure or temperature, or capping agents. In the precipitation reaction, upon the slow addition of a strong alkali (in our case NaOH), the reaction pH increased to 10, and a pinkish-white precipitate was

formed. This precipitate could be easily collected by centrifugation, and the color turned yellowish upon drying.

Both nanoparticles were annealed at 400 °C for 4 h. The selected annealing temperature was proven not to alter the particle size or the crystalline nature of the formed nanoparticles [46]. GeO<sub>2</sub>NPs were quasi-spherical in shape with a diameter of 20 nm. In contrast to the previous study of Nejaty-Moghadam and his colleagues [28], we changed the reaction duration from 30 min to 4 h, and the reaction temperature was raised to 150 °C instead of 50 °C while maintaining a 4:1 ratio between acetylacetone and germanium tetrachloride. In the case of CeO<sub>2</sub>NPs, the produced nanoparticles were 12–15 nm in diameter, as reported earlier [47] with a spherical shape.

The nanoparticles were crystalline and GeO<sub>2</sub>NPs showed a pure hexagonal phase. This alpha quartz-like hexagonal structure is known for its stability at high temperatures and pressure [48]. The obtained XRD pattern is in line with previous studies [19,28]. CeO<sub>2</sub>NPs showed a face-lefted cubic phase. Based on oxygen niche, there are various phases of CeO<sub>2</sub>NPs, including fluorite, bixbyite, rhombohedral, and triclinic phases [49]. Based on XRD results, our synthesized CeO<sub>2</sub>NPs had a pure fluorite phase. This phase structure allows for redox cycles and this explains the prominent antioxidant activity of CeO<sub>2</sub>NPs [50]. The fabrication of both nanoparticles was confirmed by FTIR analysis, where characteristic absorption peaks for GeO<sub>2</sub>NPs at 870 cm<sup>-1</sup> and CeO<sub>2</sub>NPs at 857 cm<sup>-1</sup> were present. Chemisorbed molecules on the surface, such as water and bicarbonate, were also observed. They provide the hydroxyl groups through which fabricated nanoparticles can interact with other molecules, such as carbohydrates [51].

The surface charge of the nanoparticles performs a vital role in their pharmacokinetic profile. The overall charge determines the interaction with carrier proteins (e.g., albumin), cellular uptake, and subcellular distribution [52]. GeO<sub>2</sub>NPs zeta potential was −27 mV while it was −17 mV for CeO<sub>2</sub>NPs as an average surface charge. Bearing a negative charge increases the repulsive forces between the nanoparticles and fosters the formation of stable colloidal suspensions [53].

Many studies showed that AD is linked with oxidative stress. Generated radicals cause lipid peroxidation, protein oxidation, DNA damage, and glycooxidation within the brain tissues. Deficiency of antioxidants and prolonged oxidative stress cause neurodegeneration [54]. Accordingly, antioxidants, such as vitamin C, and vitamin E, are strongly recommended as AD therapies [55]. CeO<sub>2</sub>NPs are well reported for their antioxidant activity and redox behavior, which explained the obtained results of our conducted DPPH and APTS assays [56]. It was reported before that organogermanium could protect human dermal cells from oxidative-stress-induced cell death through the regulation of cell death and inflammatory genes [57] and its administration elevated the antioxidant levels of treated rats [58]. Our study showed that GeO<sub>2</sub>NPs exerted radical scavenging activity in a dose-dependent manner and their activity was stronger than CeO<sub>2</sub>NPs at concentrations above 60 µg/mL. This finding was confirmed by both DPPH and APTS assays and it is worth mentioning that this is the first report on this activity.

The doses of GeO<sub>2</sub>NPs and CeO<sub>2</sub>NPs administered to the rats were proven to be safe. They have improved the redox status of the animals as indicated by the significant increase in the GSH and SOD levels compared to the control. This might be attributed to the activation of Nrf-2 pathway. While AD cannot be cured, boosting the brain antioxidant status is desirable and reported as a prophylactic practice to AD and other neurodegenerative diseases [59].

In the present research, the AD model was established and treated with either CeO<sub>2</sub>NPs or GeO<sub>2</sub>NPs. Treatment efficiency was assessed by measuring the serum and tissue tau protein, phosphorylated tau, neurogranin (NG), Aβ peptide 1-42, Acetylcholinesterase (AChE), and monoamine oxidase (MAO). Our findings indicated that GeO<sub>2</sub>NPs were superior to CeO<sub>2</sub>NPs since they restored biomarker levels almost to the control values. Those findings agreed with their radical scavenging activity results and thus might be related to their antioxidant activity.

A variety of new biomarkers for early diagnosis of AD have emerged in recent years. The level of neurogranin (NG) in cerebrospinal fluid (CSF) showed a positive correlation with total tau and phosphorylated tau protein in CSF in AD patients. Tau is the main neuronal microtubule protein in the brain of AD patients; it is abnormally hyperphosphorylated and aggregated into paired helical filaments, which appear as neurofibrillary tangles (NFTs). This suggests that tau protein may be a promising target for developing therapeutic medications for AD [60].

Tau primarily functions by stimulating microtubule assembly and stabilizing the microtubule structure and its phosphorylation state regulates this function. Normal brain tau contains two to three moles of phosphate per mole [61]. In AD brains, Tau is abnormally hyperphosphorylated and the result is the major subunit of paired helical filaments (PHFs) and straight filaments (SFs), which form NFTs, neuropil threads, and plaque dystrophic neurites. Tau hyperphosphorylation appears to result in neurofibrillary degeneration in AD [60]. These results strongly support our findings regarding tau and phospho tau levels.

It has been shown that the number of NFTs, not the presence of plaques, correlates most closely with the degree and/or presence of dementia in AD. It appears that neurofibrillary degeneration is necessary for the clinical manifestation of the disease. Depending on the molecular mechanism of tau-mediated neurofibrillary degeneration, therapeutic strategies may include increased tau clearance, inhibition of abnormal tau hyperphosphorylation, and suppression of tau misfolding/aggregation [60].

Neurogranin (NG) is a post-synaptic protein that is especially abundant in the dendritic spines of the hippocampus, amygdala, caudate, and putamen. It binds the calcium-binding protein calmodulin (CaM) to modulate calcium signaling and synaptic plasticity [62]. NG has a vital role in the initiation of long-term potentiation (LTP) in the hippocampus. In the normal human brain, NG expression is the highest in associative cortical areas, while in AD, NG levels are depleted in the cortex and hippocampus, reflecting synaptic loss [63]. Studies of blood NG are limited, and they have not described significant variations between AD and controls [64].

In animal models, NG knockdown restrains synaptic LTP and affects mental capacity, while NG up-regulation advances LTP and further develops cognition. Comparative investigations are accounted for in patients with AD, as NG is depleted in the brain and this exhaustion is related to more unfortunate mental performance. NG can identify the neurotic changes of AD at prior stages, even in the mild cognitive impairment (MCI) stage, and subsequently is viewed as a potential biomarker for the determination of AD [65].

The level of NG in blood plasma exosomes of patients with AD and MCI was low compared to controls, and NG levels in blood plasma exosomes of patients with AD and MCI-AD were also lower than those in patients with MCI. These findings emphasized the clinical proof that NG in blood exosomes can be used as a cognitive biomarker for AD and MCI [66]. Kvartsberg et al. [67] reported that the level of NG in the blood plasma exosomes was the same as that of AD patient brain tissues, but the level in the CSF was the reverse. Liu et al. [66] hypothesized that the raise of NG level in CSF and the decline of NG in blood plasma exosomes and brain tissues in patients with AD and MCI-AD were related to the decomposition of NG into many peptides modified by disulfide bridges or glutathione and released into CSF.

Unlike the biochemical pathway of A $\beta$  and tau, NG acts in response to synaptic loss or synaptic plasticity disorder. Synaptic dysfunction and deterioration are believed to be central issues in AD pathology from early stages because learning and memory are formed through synaptic plasticity [68]. This evidence reveals that NG can be an encouraging factor for the early identification of cognitive deterioration. NG binding to CaM weakens when the synaptic structure is interrupted, affecting the diffusion of Ca<sup>2+</sup> between the synapses and the formation of LTP, leading to early cognitive decline. More significantly, studies in humans have shown that expression of NG declined in the frontal and parietal cortices of AD patients, and NG was significantly correlated with the degree of amyloid and tau pathology [66].

Acetylcholinesterase (AChE) is a catalytic enzyme responsible for the breakdown of the acetylcholine. Since AD can be regarded as a loss of cholinergic neurons, reducing AChE is a reasonable modality. Additionally, AChE is known to act as an amyloidogenic factor supporting the deposition of tau protein and augmenting its correlated neurotoxicity [69].

Monoamines assume a huge part in cognition managing memory and learning. Abnormal monoaminergic signaling generally goes with cholinergic deficiencies, which supports early phase changes in monoaminergic tone, compounded by cholinergic deficits, as contributing elements to the mental deterioration in AD [70]. Specific changes in monoaminergic capacity could be a significant contributor to neuropsychiatric symptoms, including depression, irritability, aggressive outbursts, and delusions [71]. Notably, these diseases reflect region-specific noradrenergic and serotonergic insults; in this way, MAO-A and MAO-B dysfunction, and a monoaminergic injury, could participate to a spectrum of symptoms and pathology in both early and sustained AD development [70].

MAO may also be a factor in neuropathology because of the generation of hydrogen peroxide as a by-product of the deamination reaction. The ensuing oxidative stress and potential for cell death—invariably involving the mitochondria—would be exacerbated when antioxidant systems are compromised as in the case of AD [72]. AD subjects usually show an increase in MAO-B in the brain and platelets. Studies demonstrated an increased binding of the MAO-B-specific ligand 11C-deuterium-L-deprenyl (11C-DED) early in pre-symptomatic Familial Alzheimer's Disease (FAD) cases, which was thought to boost astrocytosis. Nevertheless, the mechanism by which MAO-B affects AD pathogenesis is not known. Some initial outcomes suggest that MAO-B is correlated with  $\gamma$ -secretase activity [73].

In the present study, CeO<sub>2</sub>NPs and GeO<sub>2</sub>NPs significantly improved tau and phospho tau protein through their antioxidant effect. Dowding et al. [14] stated that 2.9 nm citrate/EDTA-stabilized CeO<sub>2</sub>NPs administered intravenously to healthy rats seem to cross the intact blood-brain barrier (BBB). By contrast, another study by Kim et al. [74] used phospholipid-polyethylene glycol-coated CeO<sub>2</sub>NPs, yet these particles were found only in low amounts in normal brain tissue. In AD cases, BBB is dysfunctional, thus nanoparticles are more likely to adequately present within brain tissues [75].

In vitro and in vivo, CeO<sub>2</sub>NPs demonstrated antioxidant properties due to their superoxide dismutase (SOD) and catalase (CAT)-like activities. In general, CeO<sub>2</sub>NPs remove ROS due to surface self-regeneration [76]. However, the excessive generation of ROS found in neurodegenerative diseases can harm cells, necessitating exogenous aids. Considering this, antioxidants are frequently used. On the other hand, antioxidants are unable to cross the BBB, emphasizing the importance of nanoparticle-based antioxidant delivery systems [77]. CeO<sub>2</sub>NPs, which continually scavenge ROS, are of such delivery systems.

CeO<sub>2</sub>NPs have been proposed by Naz et al. [15] as a potential treatment candidate for mitochondrial injury. When compared to other ROS modulators, CeO<sub>2</sub>NP's unique redox behavior makes it a strong antioxidant. CeO<sub>2</sub>NPs can modify the brain-derived neurotrophic factor signal transduction pathway in AD, retarding the apoptotic effect of the disease in neuronal cells. When conjugated with metal chelators or polyethylene glycol coatings, they can reduce A $\beta$  aggregation [78]. Studies have also shown that CeO<sub>2</sub>NPs inhibited A $\beta$ -mediated mitochondrial fragmentation via a mechanism involving the decrease in DRP1 S616 hyperphosphorylation [14]. Although it is doubtful that nitrosative stress causes mitochondrial breakage and neuronal cell death by phosphorylating a single protein target, such as DRP1, these findings describe one possible mechanism by which CeO<sub>2</sub>NPs can mitigate the downstream effects of RNS/ROS. Before moving on to human therapeutic trials, more in vitro and in vivo investigations are needed.

On the molecular level, miRNAs have frequently been found to be disorganized in AD. Many miRNAs have been identified as important factors in the regulation of cognitive functioning and memory processes lost in AD [79]. As a result, distinct miRNAs may perform a protective or promoting function in AD. In the current study, the expression of nine miRNAs was investigated in brain tissue. Among the tested miRNAs, miR-29a-3p,

a well-known brain-enriched miRNA, is considered to be a potential biomarker for AD, especially from CSF, as it is significantly increased in AD patients compared to controls. In vitro, it was evident that miR-29a-3p can regulate beta-site APP-cleaving enzyme (BACE) expression. Moreover, miR-29a-3p has potentially been involved in the up-regulation of amyloid precursor protein and BACE1 expression. In contrast, Hébert and his team [6] stated that the miR-29a is significantly decreased in AD patients displaying abnormally high BACE1 protein. It is not clear whether this correlation of miR-29a-3p/BACE expression is restricted to certain areas of the brain or broadly expressed. In the current investigation, miR-29a-3p was shown to indicate a successful therapeutic response using GeO<sub>2</sub>NPs.

## 5. Conclusions

Based on the gathered data, GeO<sub>2</sub>NPs and CeO<sub>2</sub>NPs are emerging as promising new tools to be authenticated as possible pharmacological treatments in neurodegenerative diseases, especially AD. The validation of new therapeutic agents suggests the understanding of their mechanisms of action; therefore, we report the effects of GeO<sub>2</sub>NPs and CeO<sub>2</sub>NPs on tau and phospho tau proteins, A $\beta$  peptide 1-42, and neurogranin, acetylcholinesterase, and monoamine oxidase, all known to be engaged in neuronal survival. The results obtained strongly support a neurotrophic role for these nanoparticles and indicate their use as a modulator of pathways crucial for neuronal survival.

**Supplementary Materials:** The following supporting information can be downloaded at: <https://www.mdpi.com/article/10.3390/pharmaceutics15051386/s1>, Figure S1: (a) antioxidant activity of GeO<sub>2</sub>NPs and CeO<sub>2</sub>NPs tested by DPPH assay, (b) antioxidant activity of GeO<sub>2</sub>NPs and CeO<sub>2</sub>NPs tested by APTS assay. Vitamin C (Vit. C) was used as a standard.

**Author Contributions:** Conceptualization, S.A.A.G., A.H.H., M.A.T., E.A.T. and H.H.A.; methodology, S.A.A.G., A.H.H., M.A.T., E.A.T. and H.H.A.; formal analysis, S.A.A.G., A.H.H., M.A.T., E.A.T. and H.H.A.; investigation, S.A.A.G., A.H.H., M.A.T., E.A.T. and H.H.A.; writing—original draft preparation, S.A.A.G., A.H.H., M.A.T., E.A.T. and H.H.A.; writing—review and editing, S.A.A.G. All authors have read and agreed to the published version of the manuscript.

**Funding:** This research received no external funding.

**Institutional Review Board Statement:** The study was conducted in accordance with the Declaration of Helsinki and approved by the Ethical Committee for Medical Research of the National Research Centre, Egypt obtained in July 2021 with the approval number 1416072021.

**Informed Consent Statement:** Not applicable.

**Data Availability Statement:** Data are available upon request from the corresponding author.

**Acknowledgments:** A sincere thanks to Loula Burton from Tulane's Research Proposal Development Office for her diligent editing and proofreading of this manuscript.

**Conflicts of Interest:** The authors declare no conflict of interest.

## References

1. Sikorska, K.; Grądzka, I.; Sochanowicz, B.; Presz, A.; Męczyńska-Wielgosz, S.; Brzóška, K.; Kruszewski, M.K. Diminished amyloid- $\beta$  uptake by mouse microglia upon treatment with quantum dots, silver or cerium oxide nanoparticles: Nanoparticles and amyloid- $\beta$  uptake by microglia. *Hum. Exp. Toxicol.* **2020**, *39*, 147–158. [[CrossRef](#)]
2. Choubdar, N.; Avizheh, S. Nanotechnology Based Delivery Systems of Drugs Currently Used to Treat Alzheimer's Disease. *Nanosci. Nanotechnol.-Asia* **2020**, *10*, 228–247. [[CrossRef](#)]
3. Dregni, A.J.; Duan, P.; Xu, H.; Changolkar, L.; El Mammeri, N.; Lee, V.M.-Y.; Hong, M. Fluent molecular mixing of Tau isoforms in Alzheimer's disease neurofibrillary tangles. *Nat. Commun.* **2022**, *13*, 2967. [[CrossRef](#)] [[PubMed](#)]
4. Uddin, M.S.; Stachowiak, A.; Al Mamun, A.; Tzvetkov, N.T.; Takeda, S.; Atanasov, A.G.; Bergantin, L.B.; Abdel-Daim, M.M.; Stankiewicz, A.M. Autophagy and Alzheimer's Disease: From Molecular Mechanisms to Therapeutic Implications. *Front. Aging Neurosci.* **2018**, *10*, 4. [[CrossRef](#)] [[PubMed](#)]
5. Turner, R.S.; Stubbs, T.; Davies, D.A.; Albeni, B.C. Potential New Approaches for Diagnosis of Alzheimer's Disease and Related Dementias. *Front. Neurol.* **2020**, *11*, 496. [[CrossRef](#)]

6. Hébert, S.S.; Horré, K.; Nicolai, L.; Papadopoulou, A.S.; Mandemakers, W.; Silahatoglu, A.N.; Kauppinen, S.; Delacourte, A.; De Strooper, B. Loss of microRNA cluster miR-29a/b-1 in sporadic Alzheimer's disease correlates with increased BACE1/beta-secretase expression. *Proc. Natl. Acad. Sci. USA* **2008**, *105*, 6415–6420. [[CrossRef](#)] [[PubMed](#)]
7. Angelucci, F.; Cechova, K.; Valis, M.; Kuca, K.; Zhang, B.; Hort, J. MicroRNAs in Alzheimer's Disease: Diagnostic Markers or Therapeutic Agents? *Front. Pharmacol.* **2019**, *10*, 665. [[CrossRef](#)] [[PubMed](#)]
8. Swarbrick, S.; Wragg, N.; Ghosh, S.; Stolzing, A. Systematic Review of miRNA as Biomarkers in Alzheimer's Disease. *Mol. Neurobiol.* **2019**, *56*, 6156–6167. [[CrossRef](#)]
9. Jaber, V.R.; Zhao, Y.; Sharfman, N.M.; Li, W.; Lukiw, W.J. Addressing Alzheimer's Disease (AD) Neuropathology Using Anti-microRNA (AM) Strategies. *Mol. Neurobiol.* **2019**, *56*, 8101–8108. [[CrossRef](#)] [[PubMed](#)]
10. Cosín-Tomás, M.; Alvarez-López, M.; Sanchez-Roige, S.; Lalanza, J.; Bayod, S.; Sanfeliu, C.; Pallas, M.; Escorihuela, R.; Kaliman, P. Epigenetic alterations in hippocampus of SAMP8 senescent mice and modulation by voluntary physical exercise. *Front. Aging Neurosci.* **2014**, *6*, 51. [[CrossRef](#)]
11. Zhou, H.; Zhang, R.; Lu, K.; Yu, W.; Xie, B.; Cui, D.; Jiang, L.; Zhang, Q.; Xu, S. Deregulation of miRNA-181c potentially contributes to the pathogenesis of AD by targeting collapsin response mediator protein 2 in mice. *J. Neurol. Sci.* **2016**, *367*, 3–10. [[CrossRef](#)]
12. Birks, J. Cholinesterase inhibitors for Alzheimer's disease. *Cochrane Database Syst. Rev.* **2006**, *2006*, CD005593. [[CrossRef](#)] [[PubMed](#)]
13. D'Angelo, B.; Santucci, S.; Benedetti, E.; Di Loreto, S.; Phani, A.R.; Falone, S.; Amicarelli, F.; Ceru, P.M.; Cimini, A. Cerium Oxide Nanoparticles Trigger Neuronal Survival in a Human Alzheimer Disease Model By Modulating BDNF Pathway. *Curr. Nanosci.* **2009**, *5*, 167–176. [[CrossRef](#)]
14. Dowding, J.M.; Song, W.; Bossy, K.; Karakoti, A.; Kumar, A.; Kim, A.; Bossy, B.; Seal, S.; Ellisman, M.H.; Perkins, G.; et al. Cerium oxide nanoparticles protect against A $\beta$ -induced mitochondrial fragmentation and neuronal cell death. *Cell Death Differ.* **2014**, *21*, 1622–1632. [[CrossRef](#)] [[PubMed](#)]
15. Naz, S.; Beach, J.; Heckert, B.; Tummala, T.; Pashchenko, O.; Banerjee, T.; Santra, S. Cerium oxide nanoparticles: A "radical" approach to neurodegenerative disease treatment. *Nanomedicine* **2017**, *12*, 545–553. [[CrossRef](#)] [[PubMed](#)]
16. Dobrzyński, D.; Boguszewska-Czubara, A.; Sugimori, K. Hydrogeochemical and biomedical insights into germanium potential of curative waters: A case study of health resorts in the Sudetes Mountains (Poland). *Environ. Geochem. Health* **2018**, *40*, 1355–1375. [[CrossRef](#)] [[PubMed](#)]
17. Cho, J.M.; Chae, J.; Jeong, S.R.; Moon, M.J.; Shin, D.Y.; Lee, J.H. Immune activation of Bio-Germanium in a randomized, double-blind, placebo-controlled clinical trial with 130 human subjects: Therapeutic opportunities from new insights. *PLoS ONE* **2020**, *15*, e0240358. [[CrossRef](#)]
18. Furst, A. Biological testing of germanium. *Toxicol. Ind. Health* **1987**, *3*, 167–204. [[CrossRef](#)]
19. Bioud, Y.A.; Paradis, E.; Boucherif, A.; Drouin, D.; Arès, R. Shape control of cathodized germanium oxide nanoparticles. *Electrochem. Commun.* **2021**, *122*, 106906. [[CrossRef](#)]
20. Chen, X.; Cai, Q.; Zhang, J.; Chen, Z.; Wang, W.; Wu, Z.; Wu, Z. Synthesis and growth of germanium oxide nanoparticles in AOT reversed micelle. *Mater. Lett.* **2007**, *61*, 535–537. [[CrossRef](#)]
21. Kim, W.J.; Soshnikova, V.; Markus, J.; Oh, K.H.; Anandapadmanaban, G.; Mathiyalagan, R.; Perez, Z.E.J.; Kim, Y.J.; Yang, D.C. Room temperature synthesis of germanium dioxide nanorods and their in vitro photocatalytic application. *Optik* **2019**, *178*, 664–668. [[CrossRef](#)]
22. Dhenadhayan, N.; Chauhan, A.; Lin, K.-C.; Alfantazi, A. Architecting 3D prism shaped carbon dots/germanium/germanium oxide nanohybrid for photocatalytic degradation of pendimethalin and dinotefuran pesticides. *Mater. Today Chem.* **2022**, *24*, 100913. [[CrossRef](#)]
23. Lin, M.-H.; Hsu, T.-S.; Yang, P.-M.; Tsai, M.-Y.; Perng, T.-P.; Lin, L.-Y. Comparison of organic and inorganic germanium compounds in cellular radiosensitivity and preparation of germanium nanoparticles as a radiosensitizer. *Int. J. Radiat. Biol.* **2009**, *85*, 214–226. [[CrossRef](#)] [[PubMed](#)]
24. Zhang, W.; Pang, H.; Sun, W.; Lv, L.-P.; Wang, Y. Metal-organic frameworks derived germanium oxide nanosheets for large reversible Li-ion storage. *Electrochem. Commun.* **2017**, *84*, 80–85. [[CrossRef](#)]
25. Li, D.; Wang, H.; Liu, H.K.; Guo, Z. A New Strategy for Achieving a High Performance Anode for Lithium Ion Batteries—Encapsulating Germanium Nanoparticles in Carbon Nanoboxes. *Adv. Energy Mater.* **2016**, *6*, 1501666. [[CrossRef](#)]
26. Lobaz, V.; Rabyk, M.; Pánek, J.; Doris, E.; Nallet, F.; Štěpánek, P.; Hrubý, M. Photoluminescent polysaccharide-coated germanium(IV) oxide nanoparticles. *Colloid Polym. Sci.* **2016**, *294*, 1225–1235. [[CrossRef](#)]
27. Riabinina, D.; Durand, C.; Chaker, M.; Rowell, N.; Rosei, F. A novel approach to the synthesis of photoluminescent germanium nanoparticles by reactive laser ablation. *Nanotechnology* **2006**, *17*, 2152–2155. [[CrossRef](#)]
28. Nejaty-Moghadam, L.; Esmaili-Bafghi-Karimabad, A.; Gholamrezaei, S.; Hamadian, M.; Salavati-Niasari, M. Facile synthesis of GeO<sub>2</sub> nanostructures and measurement of photocatalytic, photovoltaic and photoluminescence properties. *J. Mater. Sci. Mater. Electron.* **2015**, *26*, 6386–6394. [[CrossRef](#)]

29. Chouaib, F.; Delgado, G.; Beaunier, P.; Picard, G. Characterization of cerium oxides prepared in water and sodium hydroxide mixtures. *J. Alloys Compd.* **1992**, *185*, 279–293. [[CrossRef](#)]
30. Aboelmaati, M.G.; Abdel Gaber, S.A.; Soliman, W.E.; Elkhatib, W.F.; Abdelhameed, A.M.; Sahyon, H.A.; El-Kemary, M. Biogenic and biocompatible silver nanoparticles for an apoptotic anti-ovarian activity and as polydopamine-functionalized antibiotic carrier for an augmented antibiofilm activity. *Colloids Surf. B. Biointerfaces* **2021**, *206*, 111935. [[CrossRef](#)]
31. Aseyd Nezhad, S.; Es-haghi, A.; Tabrizi, M.H. Green synthesis of cerium oxide nanoparticle using *Origanum majorana* L. leaf extract, its characterization and biological activities. *Appl. Organomet. Chem.* **2020**, *34*, e5314. [[CrossRef](#)]
32. Turin-Moleavin, I.-A.; Fifere, A.; Lungoci, A.-L.; Rosca, I.; Coroaba, A.; Peptanariu, D.; Pasca, S.-A.; Bostanaru, A.-C.; Mares, M.; Pinteala, M. In Vitro and In Vivo Antioxidant Activity of the New Magnetic-Cerium Oxide Nanoconjugates. *Nanomaterials* **2019**, *9*, 1565. [[CrossRef](#)] [[PubMed](#)]
33. Sanai, T.; Onoyama, K.; Osato, S.; Motomura, K.; Oochi, N.; Oh, Y.; Okuda, S.; Takaichi, S.; Fujishima, M. Dose Dependency of Germanium-Dioxide-Induced Nephrotoxicity in Rats. *Nephron* **1991**, *57*, 349–354. [[CrossRef](#)] [[PubMed](#)]
34. El Shaer, S.S.; Salaheldin, T.A.; Saied, N.M.; Abdelazim, S.M. In vivo ameliorative effect of cerium oxide nanoparticles in isoproterenol-induced cardiac toxicity. *Exp. Toxicol. Pathol.* **2017**, *69*, 435–441. [[CrossRef](#)] [[PubMed](#)]
35. Sawy, A.M.; Barhoum, A.; Abdel Gaber, S.A.; El-Hallouty, S.M.; Shousha, W.G.; Maarouf, A.A.; Khalil, A.S.G. Insights of doxorubicin loaded graphene quantum dots: Synthesis, DFT drug interactions, and cytotoxicity. *Mater. Sci. Eng. C* **2021**, *122*, 111921. [[CrossRef](#)]
36. Abdel Khalek, M.A.; Abdel Gaber, S.A.; El-Domany, R.A.; El-Kemary, M.A. Photoactive electrospun cellulose acetate/polyethylene oxide/methylene blue and trilayered cellulose acetate/polyethylene oxide/silk fibroin/ciprofloxacin nanofibers for chronic wound healing. *Int. J. Biol. Macromol.* **2021**, *193*, 1752–1766. [[CrossRef](#)]
37. Fadl, N.N.; Ahmed, H.H.; Booles, H.F.; Sayed, A.H. Serrapeptase and nattokinase intervention for relieving Alzheimer's disease pathophysiology in rat model. *Hum. Exp. Toxicol.* **2013**, *32*, 721–735. [[CrossRef](#)]
38. Tsakiris, S.; Carageorgiou, H.; Schulpis, K.H. The Protective Effect of L-Cysteine and Glutathione on the Adult and Aged Rat Brain ( $\text{Na}^+$ ,  $\text{K}^+$ )-ATPase and  $\text{Mg}^{2+}$ -ATPase Activities in Galactosemia In Vitro. *Metab. Brain Dis.* **2005**, *20*, 87–95. [[CrossRef](#)]
39. Lowry, O.H.; Rosebrough, N.J.; Farr, A.L.; Randall, R.J. Protein measurement with the Folin phenol reagent. *J. Biol. Chem.* **1951**, *193*, 265–275. [[CrossRef](#)]
40. Preusse, M.; Tantawy, M.A.; Klawonn, F.; Schughart, K.; Pessler, F. Infection- and procedure-dependent effects on pulmonary gene expression in the early phase of influenza A virus infection in mice. *BMC Microbiol.* **2013**, *13*, 293. [[CrossRef](#)]
41. Petersen, H.; Mostafa, A.; Tantawy, M.A.; Iqbal, A.A.; Hoffmann, D.; Tallam, A.; Selvakumar, B.; Pessler, F.; Beer, M.; Rautenschlein, S.; et al. NS Segment of a 1918 Influenza A Virus-Descendent Enhances Replication of H1N1pdm09 and Virus-Induced Cellular Immune Response in Mammalian and Avian Systems. *Front. Microbiol.* **2018**, *9*, 526. [[CrossRef](#)] [[PubMed](#)]
42. Thakur, N.; Manna, P.; Das, J. Synthesis and biomedical applications of nanoceria, a redox active nanoparticle. *J. Nanobiotechnology* **2019**, *17*, 84. [[CrossRef](#)]
43. Thakur, S.; Patil, P. Rapid synthesis of cerium oxide nanoparticles with superior humidity-sensing performance. *Sensors Actuators B Chem.* **2014**, *194*, 260–268. [[CrossRef](#)]
44. Goharshadi, E.K.; Samiee, S.; Nancarrow, P. Fabrication of cerium oxide nanoparticles: Characterization and optical properties. *J. Colloid Interface Sci.* **2011**, *356*, 473–480. [[CrossRef](#)] [[PubMed](#)]
45. Yin, L.; Wang, Y.; Pang, G.; Koltypin, Y.; Gedanken, A. Sonochemical synthesis of cerium oxide nanoparticles-effect of additives and quantum size effect. *J. Colloid Interface Sci.* **2002**, *246*, 78–84. [[CrossRef](#)] [[PubMed](#)]
46. Tolasz, J.; Henych, J.; Šřastný, M.; Němečková, Z.; Slušná, M.Š.; Opletal, T.; Janoš, P. Room-temperature synthesis of nanoceria for degradation of organophosphate pesticides and its regeneration and reuse. *RSC Adv.* **2020**, *10*, 14441–14450. [[CrossRef](#)]
47. Baalousha, M.; Ju-Nam, Y.; Cole, P.A.; Gaiser, B.; Fernandes, T.F.; Hriljac, J.A.; Jepson, M.A.; Stone, V.; Tyler, C.R.; Lead, J.R. Characterization of cerium oxide nanoparticles-part 1: Size measurements. *Environ. Toxicol. Chem.* **2012**, *31*, 983–993. [[CrossRef](#)]
48. Nabata, H.; Takagi, M.; Saita, K.; Maeda, S. Computational searches for crystal structures of dioxides of group 14 elements ( $\text{CO}_2$ ,  $\text{SiO}_2$ ,  $\text{GeO}_2$ ) under ultrahigh pressure. *RSC Adv.* **2020**, *10*, 22156–22163. [[CrossRef](#)]
49. Bekheet, M.F.; Grünbacher, M.; Schlicker, L.; Gili, A.; Doran, A.; Epping, J.D.; Gurlo, A.; Klötzer, B.; Penner, S. On the structural stability of crystalline ceria phases in undoped and acceptor-doped ceria materials under in situ reduction conditions. *CrystEngComm* **2019**, *21*, 145–154. [[CrossRef](#)]
50. Li, C.; Shi, X.; Shen, Q.; Guo, C.; Hou, Z.; Zhang, J. Hot Topics and Challenges of Regenerative Nanoceria in Application of Antioxidant Therapy. *J. Nanomater.* **2018**, *2018*, 4857461. [[CrossRef](#)]
51. Milenković, I.; Mitrović, A.; Algarra, M.; Lázaro-Martínez, J.M.; Rodríguez-Castellón, E.; Maksimović, V.; Spasić, S.Z.; Beškoski, V.P.; Radotić, K. Interaction of Carbohydrate Coated Cerium-Oxide Nanoparticles with Wheat and Pea: Stress Induction Potential and Effect on Development. *Plants* **2019**, *8*, 478. [[CrossRef](#)] [[PubMed](#)]
52. Fröhlich, E. The role of surface charge in cellular uptake and cytotoxicity of medical nanoparticles. *Int. J. Nanomed.* **2012**, *7*, 5577–5591. [[CrossRef](#)] [[PubMed](#)]
53. Rasmussen, M.K.; Pedersen, J.N.; Marie, R. Size and surface charge characterization of nanoparticles with a salt gradient. *Nat. Commun.* **2020**, *11*, 2337. [[CrossRef](#)] [[PubMed](#)]

54. Gella, A.; Durany, N. Oxidative stress in Alzheimer disease. *Cell Adh. Migr.* **2009**, *3*, 88–93. [[CrossRef](#)]
55. Feng, Y.; Wang, X. Antioxidant therapies for Alzheimer's disease. *Oxid. Med. Cell. Longev.* **2012**, *2012*, 472932. [[CrossRef](#)]
56. Karakoti, A.S.; Monteiro-Riviere, N.A.; Aggarwal, R.; Davis, J.P.; Narayan, R.J.; Self, W.T.; McGinnis, J.; Seal, S. Nanoceria as Antioxidant: Synthesis and Biomedical Applications. *JOM (1989)* **2008**, *60*, 33–37. [[CrossRef](#)]
57. Takeda, T.; Doiyama, S.; Azumi, J.; Shimada, Y.; Tokuji, Y.; Yamaguchi, H.; Nagata, K.; Sakamoto, N.; Aso, H.; Nakamura, T. Organogermanium suppresses cell death due to oxidative stress in normal human dermal fibroblasts. *Sci. Rep.* **2019**, *9*, 13637. [[CrossRef](#)]
58. Nakamura, T.; Nagura, T.; Akiba, M.; Sato, K.; Tokuji, Y.; Ohnishi, M.; Osada, K. Promotive Effects of the Dietary Organic Germanium Poly-*trans*-(2-carboxyethyl) germasesquioxane (Ge-132) on the Secretion and Antioxidative Activity of Bile in Rodents. *J. Heal. Sci.* **2010**, *56*, 72–80. [[CrossRef](#)]
59. Lee, K.H.; Cha, M.; Lee, B.H. Neuroprotective Effect of Antioxidants in the Brain. *Int. J. Mol. Sci.* **2020**, *21*, 7152. [[CrossRef](#)]
60. Gong, C.-X.; Liu, F.; Grundke-Iqbal, I.; Iqbal, K. Post-translational modifications of tau protein in Alzheimer's disease. *J. Neural Transm.* **2005**, *112*, 813–838. [[CrossRef](#)]
61. Köpke, E.; Tung, Y.C.; Shaikh, S.; Alonso, A.C.; Iqbal, K.; Grundke-Iqbal, I. Microtubule-associated protein tau. Abnormal phosphorylation of a non-paired helical filament pool in Alzheimer disease. *J. Biol. Chem.* **1993**, *268*, 24374–24384. [[CrossRef](#)] [[PubMed](#)]
62. Milà-Alomà, M.; Suárez-Calvet, M.; Molinuevo, J.L. Latest advances in cerebrospinal fluid and blood biomarkers of Alzheimer's disease. *Ther. Adv. Neurol. Disord.* **2019**, *12*, 1756286419888819. [[CrossRef](#)] [[PubMed](#)]
63. Blennow, K. A Review of Fluid Biomarkers for Alzheimer's Disease: Moving from CSF to Blood. *Neurol. Ther.* **2017**, *6*, 15–24. [[CrossRef](#)] [[PubMed](#)]
64. Olsson, B.; Lautner, R.; Andreasson, U.; Öhrfelt, A.; Portelius, E.; Bjerke, M.; Hölttä, M.; Rosén, C.; Olsson, C.; Strobel, G.; et al. CSF and blood biomarkers for the diagnosis of Alzheimer's disease: A systematic review and meta-analysis. *Lancet. Neurol.* **2016**, *15*, 673–684. [[CrossRef](#)]
65. Thorsell, A.; Bjerke, M.; Gobom, J.; Brunhage, E.; Vanmechelen, E.; Andreasen, N.; Hansson, O.; Minthon, L.; Zetterberg, H.; Blennow, K. Neurogranin in cerebrospinal fluid as a marker of synaptic degeneration in Alzheimer's disease. *Brain Res.* **2010**, *1362*, 13–22. [[CrossRef](#)]
66. Liu, W.; Lin, H.; He, X.; Chen, L.; Dai, Y.; Jia, W.; Xue, X.; Tao, J.; Chen, L. Neurogranin as a cognitive biomarker in cerebrospinal fluid and blood exosomes for Alzheimer's disease and mild cognitive impairment. *Transl. Psychiatry* **2020**, *10*, 125. [[CrossRef](#)]
67. Kvartsberg, H.; Lashley, T.; Murray, C.E.; Brinkmalm, G.; Cullen, N.C.; Höglund, K.; Zetterberg, H.; Blennow, K.; Portelius, E. The intact postsynaptic protein neurogranin is reduced in brain tissue from patients with familial and sporadic Alzheimer's disease. *Acta Neuropathol.* **2019**, *137*, 89–102. [[CrossRef](#)]
68. Casaletto, K.B.; Elahi, F.M.; Bettcher, B.M.; Neuhaus, J.; Bendlin, B.B.; Asthana, S.; Johnson, S.C.; Yaffe, K.; Carlsson, C.; Blennow, K.; et al. Neurogranin, a synaptic protein, is associated with memory independent of Alzheimer biomarkers. *Neurology* **2017**, *89*, 1782–1788. [[CrossRef](#)]
69. Rees, T.M.; Brimijoin, S. The role of acetylcholinesterase in the pathogenesis of Alzheimer's disease. *Drugs Today* **2003**, *39*, 75–83. [[CrossRef](#)]
70. Quartey, M.O.; Nyarko, J.N.K.; Pennington, P.R.; Heistad, R.M.; Klassen, P.C.; Baker, G.B.; Mousseau, D.D. Alzheimer Disease and Selected Risk Factors Disrupt a Co-regulation of Monoamine Oxidase-A/B in the Hippocampus, but Not in the Cortex. *Front. Neurosci.* **2018**, *12*, 419. [[CrossRef](#)]
71. Ritchie, K.; Lovestone, S. The dementias. *Lancet* **2002**, *360*, 1759–1766. [[CrossRef](#)] [[PubMed](#)]
72. Crack, P.J.; Cimdins, K.; Ali, U.; Hertzog, P.J.; Iannello, R.C. Lack of glutathione peroxidase-1 exacerbates Abeta-mediated neurotoxicity in cortical neurons. *J. Neural Transm.* **2006**, *113*, 645–657. [[CrossRef](#)] [[PubMed](#)]
73. Schedin-Weiss, S.; Inoue, M.; Hromadkova, L.; Teranishi, Y.; Yamamoto, N.G.; Wiehager, B.; Bogdanovic, N.; Winblad, B.; Sandebring-Matton, A.; Frykman, S.; et al. Monoamine oxidase B is elevated in Alzheimer disease neurons, is associated with  $\gamma$ -secretase and regulates neuronal amyloid  $\beta$ -peptide levels. *Alzheimers. Res. Ther.* **2017**, *9*, 57. [[CrossRef](#)] [[PubMed](#)]
74. Kim, C.K.; Kim, T.; Choi, I.-Y.; Soh, M.; Kim, D.; Kim, Y.-J.; Jang, H.; Yang, H.-S.; Kim, J.Y.; Park, H.-K.; et al. Ceria Nanoparticles that can Protect against Ischemic Stroke. *Angew. Chemie Int. Ed.* **2012**, *51*, 11039–11043. [[CrossRef](#)] [[PubMed](#)]
75. Yamazaki, Y.; Kanekiyo, T. Blood-Brain Barrier Dysfunction and the Pathogenesis of Alzheimer's Disease. *Int. J. Mol. Sci.* **2017**, *18*, 1965. [[CrossRef](#)]
76. Zand, Z.; Khaki, P.A.; Salihi, A.; Sharifi, M.; Qadir Nanakali, N.M.; Alasady, A.A.; Aziz, F.M.; Shahpasand, K.; Hasan, A.; Falahati, M. Cerium oxide NPs mitigate the amyloid formation of  $\alpha$ -synuclein and associated cytotoxicity. *Int. J. Nanomed.* **2019**, *14*, 6989–7000. [[CrossRef](#)]
77. Boonruamkaew, P.; Chonpathompikunlert, P.; Vong, L.B.; Sakaue, S.; Tomidokoro, Y.; Ishii, K.; Tamaoka, A.; Nagasaki, Y. Chronic treatment with a smart antioxidative nanoparticle for inhibition of amyloid plaque propagation in Tg2576 mouse model of Alzheimer's disease. *Sci. Rep.* **2017**, *7*, 3785. [[CrossRef](#)]

78. Cimini, A.; D'Angelo, B.; Das, S.; Gentile, R.; Benedetti, E.; Singh, V.; Monaco, A.M.; Santucci, S.; Seal, S. Antibody-conjugated PEGylated cerium oxide nanoparticles for specific targeting of A $\beta$  aggregates modulate neuronal survival pathways. *Acta Biomater.* **2012**, *8*, 2056–2067. [[CrossRef](#)]
79. Rahman, M.R.; Islam, T.; Zaman, T.; Shahjaman, M.; Karim, M.R.; Huq, F.; Quinn, J.M.W.; Holsinger, R.M.D.; Gov, E.; Moni, M.A. Identification of molecular signatures and pathways to identify novel therapeutic targets in Alzheimer's disease: Insights from a systems biomedicine perspective. *Genomics* **2020**, *112*, 1290–1299. [[CrossRef](#)]

**Disclaimer/Publisher's Note:** The statements, opinions and data contained in all publications are solely those of the individual author(s) and contributor(s) and not of MDPI and/or the editor(s). MDPI and/or the editor(s) disclaim responsibility for any injury to people or property resulting from any ideas, methods, instructions or products referred to in the content.